

Electro-osmosis modulated peristaltic flow of non-Newtonian liquid via a microchannel and variable liquid properties

R Choudhari¹, F Mebarek-Oudina², H F Öztop^{3,4*}, H Vaidya⁵ and K V Prasad⁵

¹Department of Mathematics, Karnataka State Akkamahadevi Women's University, Vijayapura, India

²Department of Physics, Faculty of Sciences, University of 20 Août 1955-Skikda, Skikda, Algeria

³Department of Medical Research, China Medical University Hospital, China Medical University, Taichung, Taiwan

⁴Department of Mechanical Engineering, Technology Faculty, Firat University, 23119 Elazig, Turkey

⁵Department of Mathematics, Vijayanagara Sri Krishnadevaraya University, Ballari, Karnataka, India

Received: 03 August 2021 / Accepted: 15 February 2022 / Published online: 14 March 2022

Abstract: A theoretical model is developed to stimulate electrokinetic transfer through peristaltic movement in a microchannel. The effect of variable viscosity, variable thermal conductivity, and wall properties is carried out. Such flows emerge in bio-mimetic pumping systems at the extremely tiny scale of significance in physiological operation, e.g., eye medication shipment systems. The sinusoidal wave-like motion propagates along the channel wall leading to the peristaltic motion. The long-wavelength and petite Reynolds number estimations are supposed to abbreviate the governing formulas. Debye–Hückel linearization is also analyzed. The variable thermal conductivity and variable viscosity parameters are used as perturbation parameters. The graphical outcomes are presented for temperature, velocity, concentration, and streamlines. Biomedical engineers can use the obtained results to create bio-microfluidic mechanisms that may assist in carrying physical liquids.

Keywords: Electro-osmosis; Debye length; Peristalsis; Variable fluid properties; Heat and mass transport; Wall properties

List of symbols

b Amplitude of the wave

T_{av} Average temperature

x Axial coordinate

K_B Boltzmann constant

Br Brinkman number

n_0 Bulk concentration

z_v Charge balance

n_2 Coefficient of viscous damping force

p Dimensionless pressure

h Displacement of the wall

E_c Eckert number

E_1 Elasticity parameter

E_x Electrical field in the x-direction

e Electronic charge

m_e Electro-osmotic parameter

(\bar{X}, \bar{Y}) Fixed frame axes

a Half width of the channel

U_{hs} Helmholtz–Smoluchowski velocity

E_2 Mass term

n_1 Mass per unit surface

S Non-dimensional shear stress

P_r Prandtl number

p_0 Pressure on the outside area of the wall due to the tension in the muscles

R_e Reynolds number

Sc Schmidt number

Sr Soret number

C_p Specific heat at constant pressure

T Temperature

K_T Thermal diffusion ratio

t Time

y Transverse coordinate

u, v Velocity components

E_3 Viscous damping force parameter

c Wave velocity

Greek letters

ϵ Amplitude ratio

Ω Concentration

λ_D Debye length

ρ Density

*Corresponding author, E-mail: hfoztop1@gmail.com

λ	Wavelength
β	Variable thermal conductivity
ϕ	Electric potential
λ_1	Jeffrey term
ψ	Stream function
α	Variable viscosity
θ	Temperature
ρ_e	Total charge density
τ	Elastic tension
ξ	Dielectric permittivity

1. Introduction

Peristalsis is a vital liquid physiological transportation mechanism in living organs. It is caused by the continuous contraction and relaxation of the vessel walls. The intestinal network, lymphatic vessels, glandular ducts, and blood vessels are all said to have peristaltic pumping as a built-in property in some cases. Peristalsis-based explorations in the industry include finger and roller pumps, the transportation of sanitary, and several corroding materials. It is used in MRIs, endoscopes, heart–lung devices, catheters, and various other bioscience applications. After Latham [1] introduced his work on peristaltic flow, scientists and researchers have used experimental, numerical, and analytical techniques to add to the literature under various assumptions and boundary conditions. In this regard, some appropriate studies have been reported in [2–10]. Peristaltic motion through a permeable medium has also gained attention due to its vast industrial and biomedical applications [11–14].

The failure of water and natural oil to fulfill the needs of thermal conductivity has created space for nanofluid research since the nanofluids enhance the thermal conductivity of conventional flow. They provide the various purposes of biomedical engineering such as drug delivery and tumor treatment and hence have become a topic of research interest [15–26].

Many industrial equipment's (control generators, heat exchange structures, MHD blowers, etc.) are based on the principle of MHD. It is also effective in drug delivery, control of blood flow during surgery, cell separation magnetic gadgets, etc. These and many more applications have promoted the study of MHD analysis in peristaltic flow [27–37]. Several articles can be found regarding the study of radiation and the MHD effect on the flow through stretching sheets [38–47]. Instead of using convective derivatives, the Jeffrey model proposes a linear simple model that uses the time derivatives and can also be

reduced to a Newtonian fluid model easily. This behavior of Jeffrey fluid exhibiting both Newtonian and non-Newtonian characteristics has attracted many researchers. The usual viscous fluid models fail to describe the stress relaxation property of non-Newtonian fluids but is well explained by the Jeffrey fluid model. The linear viscoelastic effect of Jeffrey fluid has many examples that include the dilute polymer solution thus finding numerous applications in the polymer industry. The numerous applications of Jeffrey fluid have created interest in many researchers [48–52].

One of the biggest challenges in designing microfluidic transportation systems in many of the above appliances is to make sure that the flow of liquid can be limited to the maximum amount possible. Since it does not require the typical relocating constituents attributed to usual micro-pumps, it has significant advantages in microfluidic pumping. It consents an efficient policy of microchannel motion parts using electrical fields. Electro-osmotic pumping has been discovered by affecting an electrical field to an electrolyte in contact via the surface to generate a continuous pulse-free motion. The viscous drag causes the liquid to flow tangentially toward the area, resulting in a reliable net ion migration. The strict requirement for easy-to-handle, tiny, and economical analytic mechanisms has resulted from the demand for quickly, reliable, and reputable microfluidic systems. DNA analysis/sequencing systems, chemical/biological agent discovery sensors, and drug delivery on integrated circuits are examples of such applications. In few of the above applications, one of the major challenges in the design of microfluidic transport systems is to reduce the cost of liquid movement to the lowest possible level by arranging for perfect mixes of flow activating systems. However, electro-osmosis has proven to be a simple system for creating plug-shaped like speed profiles in microchannels by controlling the statement of a pertained electrical field with free density gradients near the solid–liquid user interface. Because it does not require the typical relocating parts found in usual micro-pumps, it has significant advantages in microfluidic pumping. It allows for very reliable microchannel flow areas through electric fields. Electro-osmotic pumping has been thought to generate a continuous flow with no pulses. At the microscale, these pumps are a lot more malleable. They are widely used in pharmaceutical division, electro-osmotically activated bio-microfluidic mechanisms plasma, and splitting. Flow control is accomplished via implementing an electric field to an electrolyte in contact through a surface. The electrolyte connects the area, resulting in a web indict thickness in the remedy. The viscous drag causes the liquid to flow tangentially to the surface, resulting in a continuous ions web. Driven through the request of electro-osmotic transfer toward the peristaltic mechanism,

Chakraborty [53] proposed the peristaltic circulation with electric field. Nonetheless, a slim electrical double layer (EDL) estimation was carried. Bandopadhyay et al. [54] modified another model to review the stress circulation, channel size, and impacts of the electric field and EDL thickness. Guo and Qi [55] researched the fractional Jeffreys design of electro-osmotic peristaltic flow in a limitless microchannel to evaluate the results of electro-osmosis and fractional parameters on peristaltic circulation of fractional viscoelastic liquid. Waheed et al. [56] examined the mass and heat transport effect for EOF of a third-order drink through viscous dissipation in a microchannel. Waheed et al. [57] scrutinized the electro-osmotic modulated peristaltic flow of third-grade liquid through slip conditions. Nooren et al. [58] examined the heat qualities of an electro-osmotic phenomenon in biofluid via a peristaltic wavy microchannel. Many theoretical as well as computational researches on electro-osmotic flow with and also without heat transport have been presented [59–76].

Numerous studies conducted by considering animal physiology found that the biological liquids show variation in viscosity. The consideration is evident because the average animal or human of comparable dimensions consumes as much as two liters of water, causing a modification in the focus of physical fluids over time. Thus, considering the variation in viscosity is an essential factor while examining the peristaltic system. Ali et al. [77] inspected the effect of slip conditions over the peristaltic system and found that the pumping region diminishes for larger values of slip parameter. Nadeem et al. [78] emphasize the heat transport qualities for a third-order non-Newtonian liquid taking 2 designs of variable thickness right into account, particularly variation via temperature level and a variant through the channel's size. The nature of the walls under examination likewise plays an essential duty in the peristaltic system, and therefore, several research studies have been performed for various wall surface arrangements. In addition, the temperature variation has been revealed to transform the residential properties of the physical liquid under monitoring. Therefore, variable thermal conductivity is likewise a crucial factor to consider for the research of peristalsis for physical liquid circulations. To this end, numerous analyses have been carried out for various setups of channel wall surfaces. Temperature-dependent thermal conductivity was thought about by Hayat et al. [79] by taking Jeffrey liquid over a non-linear stretching area through variable heat change. Vaidya et al. [80] scrutinized the impact of both changeable viscosity and changeable thermal conductivity by taking Rabinowitsch liquid in a channel. Further, Manjunatha et al. [81] examined the impacts of slip conditions over the peristaltic flow of Jeffrey liquid under the consideration of different liquid properties. The studies

accounting for these properties have assisted in a better understanding of non-Newtonian fluids. Some vital researches regarding the employ of the non-Newtonian fluids in modeling and evaluation of peristaltic circulation with variable fluid properties can be found in [82–89].

The current study is the first of its kind in modeling the electrokinetically modulated peristaltic circulation of Jeffrey liquid through variable fluid properties. In addition, the effects of heat and mass transport and wall properties are considered. The governing equations are simplified through utilizing trusted estimation, namely lubrication, as well as Debye–Hückel estimate. After that, the perturbation strategy solves the resulting equation, and outcomes are contrasted numerically utilizing the MATLAB software program. The impact of relevant terms on velocity, streamlines, concentrations, and temperature is discussed graphically.

2. Mathematical formulation

2.1. Flow analysis

Consider a 2-D electrokinetic adjusted flow of Jeffrey fluid through a uniform microfluidic conduit of $2\bar{a}$ width. The propagation of sinusoidal wave shapes this flow at a continuous velocity c beside the complaint conduit walls (See Fig. 1). Let $\bar{Y} = \pm\bar{h}(\bar{X}, \bar{t})$ be the transverse displacements of the lower and upper walls, respectively. Here, propagation of wave is along the x – axis. The mass and heat transport inspection is maintained with giving T_0, C_0 and T_1, C_1 to the superior conduit wall and the inferior conduit wall, respectively. The electric field E is axially to the fluid movement.

The microchannel wall equation: [55]

$$\bar{Y} = \pm\bar{h}(\bar{X}, \bar{t}) = \pm\left(\bar{a} + \bar{b} \sin\left[2\pi\frac{(\bar{X} - c\bar{t})}{\lambda}\right]\right) \quad (1)$$

2.2. Mathematical formulations

The governing equation as given by [55] is.

Continuity equation:

$$\frac{\partial\bar{U}}{\partial\bar{X}} + \frac{\partial\bar{V}}{\partial\bar{Y}} = 0 \quad (2)$$

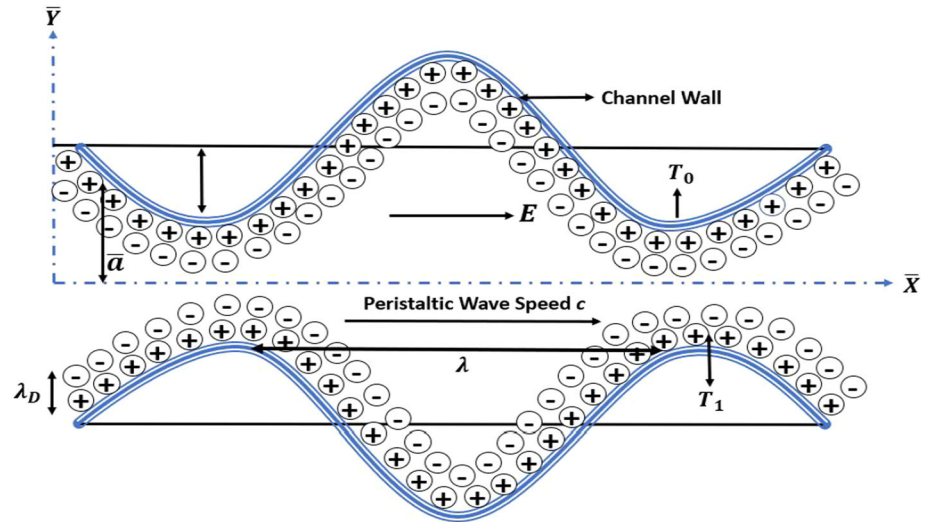
Equation of momentum:

$$\rho\left(\frac{\partial\bar{U}}{\partial\bar{t}} + \bar{U}\frac{\partial\bar{U}}{\partial\bar{X}} + \bar{V}\frac{\partial\bar{U}}{\partial\bar{Y}}\right) = -\frac{\partial\bar{P}}{\partial\bar{X}} + \frac{\partial}{\partial\bar{X}}\bar{S}_{\bar{X}\bar{X}} + \frac{\partial}{\partial\bar{Y}}\bar{S}_{\bar{X}\bar{Y}} + \rho_e E_x \quad (3)$$

$$\rho\left(\frac{\partial\bar{V}}{\partial\bar{t}} + \bar{U}\frac{\partial\bar{V}}{\partial\bar{X}} + \bar{V}\frac{\partial\bar{V}}{\partial\bar{Y}}\right) = -\frac{\partial\bar{P}}{\partial\bar{Y}} + \frac{\partial}{\partial\bar{X}}\bar{S}_{\bar{Y}\bar{X}} + \frac{\partial}{\partial\bar{Y}}\bar{S}_{\bar{Y}\bar{Y}} \quad (4)$$

Energy equation with viscous dissipation [56]

Fig. 1 Geometry of the electro-osmotic modulated peristaltic flow



$$\begin{aligned} \rho c_p \left(\frac{\partial \bar{T}}{\partial t} + \bar{U} \frac{\partial \bar{T}}{\partial \bar{X}} + \bar{V} \frac{\partial \bar{T}}{\partial \bar{Y}} \right) &= \frac{\partial}{\partial \bar{Y}} \left(k(\bar{T}) \frac{\partial \bar{T}}{\partial \bar{Y}} \right) \\ &+ \frac{\partial}{\partial \bar{X}} \left(k(\bar{T}) \frac{\partial \bar{T}}{\partial \bar{X}} \right) + \bar{S}_{\bar{X}\bar{X}} \frac{\partial \bar{U}}{\partial \bar{X}} \\ &+ \bar{S}_{\bar{Y}\bar{Y}} \frac{\partial \bar{V}}{\partial \bar{Y}} + \bar{S}_{\bar{X}\bar{Y}} \left(\frac{\partial \bar{V}}{\partial \bar{X}} + \frac{\partial \bar{U}}{\partial \bar{Y}} \right) \end{aligned} \quad (5)$$

Concentration equation:

$$\begin{aligned} \left(\frac{\partial \bar{C}}{\partial t} + \bar{U} \frac{\partial \bar{C}}{\partial \bar{X}} + \bar{V} \frac{\partial \bar{C}}{\partial \bar{Y}} \right) &= D \left(\frac{\partial^2 \bar{C}}{\partial \bar{X}^2} + \frac{\partial^2 \bar{C}}{\partial \bar{Y}^2} \right) \\ &+ \frac{DK_T}{T_m} \left(\frac{\partial^2 \bar{T}}{\partial \bar{X}^2} + \frac{\partial^2 \bar{T}}{\partial \bar{Y}^2} \right) \end{aligned} \quad (6)$$

The constitutive equation for Jeffrey fluid is: [3]

$$\bar{\tau} = -\bar{p}\bar{I} + \bar{S}, \quad \bar{S} = \frac{\mu(y)}{1 + \lambda_1} \left(\dot{\bar{\gamma}} + \lambda_2 \ddot{\bar{\gamma}} \right) \quad (7)$$

where $\bar{\tau}$ is the Cauchy stress tensor, \bar{p} is the pressure, λ_2 is the retardation time, λ_1 is the ratio of relaxation to retardation times, \bar{S} is the extra stress tensor, \bar{I} is the identity tensor, $\dot{\bar{\gamma}}$ is the shear rate, and dots over the quantities specify differentiation through time.

2.3. Electrohydrodynamics

In a microchannel, the Poisson equation is written [52] as:

$$\nabla^2 \bar{\phi} = -\frac{\rho_e}{\zeta} \quad (8)$$

here $\bar{\phi}$ denotes the electric potential, ζ is the dielectric permittivity, and ρ_e represents the total charge density.

The net charge density ρ_e follows the Boltzmann variation [59], which is

$$\rho_e = -z_v e (\bar{n}^- - \bar{n}^+) \quad (9)$$

The anions (\bar{n}^-) and cations (\bar{n}^+) are distinct by ρ_e of the Boltzmann equation:

$$\bar{n}^\pm = \bar{n}_0 e^{\left(\pm \frac{z_v e \bar{\phi}}{K_B T_{av}} \right)} \quad (10)$$

\bar{n}_0 denotes bulk concentration, K_B is the Boltzmann constant, z_v is the charge balance, e is the electronic charge, and T_{av} is the average temperature.

Employing Debye–Hückel linearization estimation [59] Eq. (8) revolves into

$$+ \frac{d^2 \phi}{dy^2} = m_e^2 \phi \quad (11)$$

where m_e represents the electro-osmotic expression. The analytical solution of Eq. (11) with boundary conditions (BCs) $\frac{\partial \phi}{\partial y} = 0$, at $y = 0$ and $\phi = 1$, at $y = h(x)$ is reached as:

$$\phi(y) = \frac{\cosh(m_e y)}{\cosh(m_e h)} \quad (12)$$

2.4. Nondimensionalization

The switch from laboratory frame (\bar{X}, \bar{Y}) to wave frame of references (\bar{x}, \bar{y}) is:

$$\begin{aligned} \bar{y} &= \bar{Y}, \quad \bar{x} = \bar{X} - c\bar{t}, \quad \bar{p}(\bar{x}, \bar{y}) = \bar{U}(\bar{X}, \bar{Y}, \bar{t}) - c \\ &= \bar{V}(\bar{X}, \bar{Y}, \bar{t}), \quad \bar{T}(\bar{x}, \bar{y}) = \bar{T}(\bar{X}, \bar{Y}, \bar{t}), \quad \bar{v}(\bar{x}, \bar{y}) \\ &= \bar{P}(\bar{X}, \bar{Y}, \bar{t}), \quad \bar{u}(\bar{x}, \bar{y}) \end{aligned} \quad (13)$$

The above conversions are employed in Eqs. (2)–(6) and then introducing the non-dimensional variables:

$$\begin{aligned}
 x &= \frac{2\pi\bar{x}}{\lambda}, y = \frac{\bar{y}}{a}, t = \frac{2\pi\bar{t}c}{\lambda}, u = \frac{\bar{u}}{c}, v = \frac{\bar{v}}{c}, p = \frac{2\pi a^2 \bar{p}}{\lambda\mu_0 c}, \\
 \alpha_1 &= \frac{2\pi a}{\lambda}, h = \frac{\bar{h}}{a}, m_e = \frac{a}{\lambda_D}, n = \frac{\bar{n}}{n_0}, f = \frac{b}{a}, \theta = \frac{\bar{T} - T_0}{T_0}, \\
 \Omega &= \frac{\bar{C} - C_0}{C_0}, \lambda_D = \frac{1}{eZ_v} \sqrt{\frac{T_0 \xi K_B}{2n_0}}, \phi = \frac{e z_v \bar{\phi}}{T_{av} K_B}, U_{hs} = -\frac{E_x \xi}{c\mu_0}, \\
 S &= \frac{a\bar{S}}{c\mu_0}, \psi = \frac{\bar{\psi}}{ca}, u = \frac{\partial\psi}{\partial y}, v = -\alpha_1 \frac{\partial\psi}{\partial x}, R_e = \frac{\rho ca}{\mu_0}, \\
 P_r &= \frac{\mu_0 c_p}{k(T)}, Br = E_c \times P_r, Sr = \frac{\rho T_0 K_T D_m}{\mu_0 T_m C_0}, Sc = \frac{\mu_0}{\rho D_m}, \\
 E_c &= \frac{c^2}{c_p T_0}, \mu_0 = \frac{\bar{\mu}_0}{\mu}, E_1 = \frac{\tau a^3}{\mu_0 \lambda^3 c}, E_2 = \frac{n_1 a^3}{\mu_0 \lambda^3 c}, E_3 = \frac{n_2 a^3}{\mu_0 \lambda^3 c}.
 \end{aligned}
 \tag{14}$$

where U_{hs} represents the Helmholtz–Smoluchowski speed, Sc is the Schmidt number, λ_D denotes the Debye length, Ω is the concentration, y is the non-dimensional transverse coordinate, m_e represents the electro-osmotic term, p is dimensionless pressure, α_1 is peristaltic wave number, P_r is the Prandtl number, θ denotes the temperature, ψ is a non-dimensional stream function, S is the non-dimensional shear stress, R_e is the Reynolds number, ϵ is the amplitude ratio, Br is the Brinkman number, Sr is the non-dimensional Soret number, x is the non-dimensional axial coordinate, and E_c is the Eckert number.

2.5. Wall properties

The governing equation of the flexible wall movement is [5]:

$$R(h) = p - p_0 \tag{15}$$

R denotes an operator, which is employed to symbolize the motion of stretched membrane via viscous damping forces such that:

$$R = -\tau \frac{\partial^2}{\partial x^2} + n_1 \frac{\partial^2}{\partial t^2} + n_2 \frac{\partial}{\partial t} \tag{16}$$

Continuity of stress at $y = h$ and employing x -momentum equation yield

$$\frac{\partial R(h)}{\partial x} = \frac{\partial p}{\partial x} = \frac{\partial}{\partial y} S_{xy} + \rho_e E_x \tag{17}$$

τ is the elastic tension in the membrane, h is the dimensional slip expression, n_1 denotes the mass per unit surface, n_2 is the coefficient of viscous damping forces, and p_0 is the pressure over the exterior surface of the wall due to the tension in the muscles. We assumed $p_0 = 0$.

The relation of the stream function ψ and the velocity is described as:

$$u = \frac{\partial\psi}{\partial y}, v = -\alpha_1 \frac{\partial\psi}{\partial x} \tag{18}$$

From Eqs. (3–6), subject to long-wavelength supposition and ignoring higher powers of α_1 , we arrive at:

$$\frac{\partial p}{\partial x} = \frac{\partial}{\partial y} \left[\left(\frac{1 - \alpha y}{1 + \lambda_1} \right) \frac{\partial^2 \psi}{\partial y^2} \right] + m_e^2 U_{hs} \phi \tag{19}$$

$$\frac{\partial p}{\partial y} = 0 \tag{20}$$

$$\frac{\partial}{\partial y} \left(k(\theta) \frac{\partial \theta}{\partial y} \right) + Br \left[\left(\frac{1 - \alpha y}{1 + \lambda_1} \right) \frac{\partial^2 \psi}{\partial y^2} \right] \frac{\partial^2 \psi}{\partial y^2} = 0, \tag{21}$$

$$\frac{\partial^2 \Omega}{\partial y^2} + Sc \times Sr \left(\frac{\partial^2 \theta}{\partial y^2} \right) = 0. \tag{22}$$

The non-dimensional boundary conditions are:

$$\frac{\partial^2 \psi}{\partial y^2} = 0, \psi = 0, \frac{\partial \theta}{\partial y} = 0, \frac{\partial \Omega}{\partial y} = 0, \text{ at } y = 0, \tag{23}$$

$$\frac{\partial \psi}{\partial y} = -1, \Omega = 0, \theta = 0 \text{ at } y = h(x) = 1 + \epsilon \sin x \tag{24}$$

The expression for variable viscosity is:

$$\mu(y) = 1 - \alpha y \text{ for } \alpha \ll 1 \tag{25}$$

The thermal conductivity term:

$$k(\theta) = 1 + \beta \theta \text{ for } \beta \ll 1 \tag{26}$$

here α denotes the viscosity coefficient, and β is the thermal conductivity coefficient.

3. Perturbation solution

Equations (19)–(22) stipulate a governing differential scheme through BCs (23) and (24) that are exceptionally non-linear. It is not possible to get an exact solution to this scheme of equations. Consequently, the scheme is solved analytically employing the perturbation technique, which utilizes α and β terms.

Hence, ψ and θ are developed as:

$$\psi = \psi_0 + \alpha \psi_1 + O(\alpha^2) \tag{27}$$

$$\theta = \theta_0 + \beta \theta_1 + O(\beta^2) \tag{28}$$

3.1. Zeroth order system

$$\frac{\partial^3 \psi_0}{\partial y^3} - (1 + \lambda_1)(P - m_e^2 U_{hs} \phi) \tag{29}$$

$$\frac{\partial \theta_0}{\partial y} = -Brf \left(\frac{1 - \alpha y \frac{\partial \psi^2}{\partial y^2}}{1 + \lambda_1 \frac{\partial \psi^2}{\partial y^2}} \right) \frac{\partial \psi^2}{\partial y^2} \quad (30)$$

Subject to these BCs

$$\psi_0 = 0, \quad \frac{\partial^2 \psi_0}{\partial y^2} = 0, \quad \frac{\partial \theta_0}{\partial y} = 0 \quad \text{at } y = 0 \quad (31)$$

$$\frac{\partial \psi_0}{\partial y} = -1, \quad \theta_0 = 0 \quad \text{at } y = h \quad (32)$$

3.2. First-order system

$$\frac{\partial^3 \psi_1}{\partial y^3} = y \frac{\partial^3 \psi_0}{\partial y^3} + \frac{\partial^2 \psi_0}{\partial y^2} \quad (33)$$

$$\frac{\partial \theta_1}{\partial y} = -\theta_0 \frac{\partial \theta_0}{\partial y} \quad (34)$$

Subject to these BCs

$$\psi_1 = 0, \quad \frac{\partial^2 \psi_1}{\partial y^2} = 0, \quad \frac{\partial \theta_1}{\partial y} = 0 \quad \text{at } y = 0 \quad (35)$$

$$\frac{\partial \psi_1}{\partial y} = 0, \quad \theta_0 = 0 \quad \text{at } y = h \quad (36)$$

The resolution of zeroth and first-order schemes along via BCs is achieved employing the MATLAB 2019b programming. The segregate code has been written to achieve the solutions for temperature, streamline, and velocity. Then, the solution for Eq. (22) is achieved by double integrating the temperature expression via the BCs (23) and (24).

4. Results and discussion

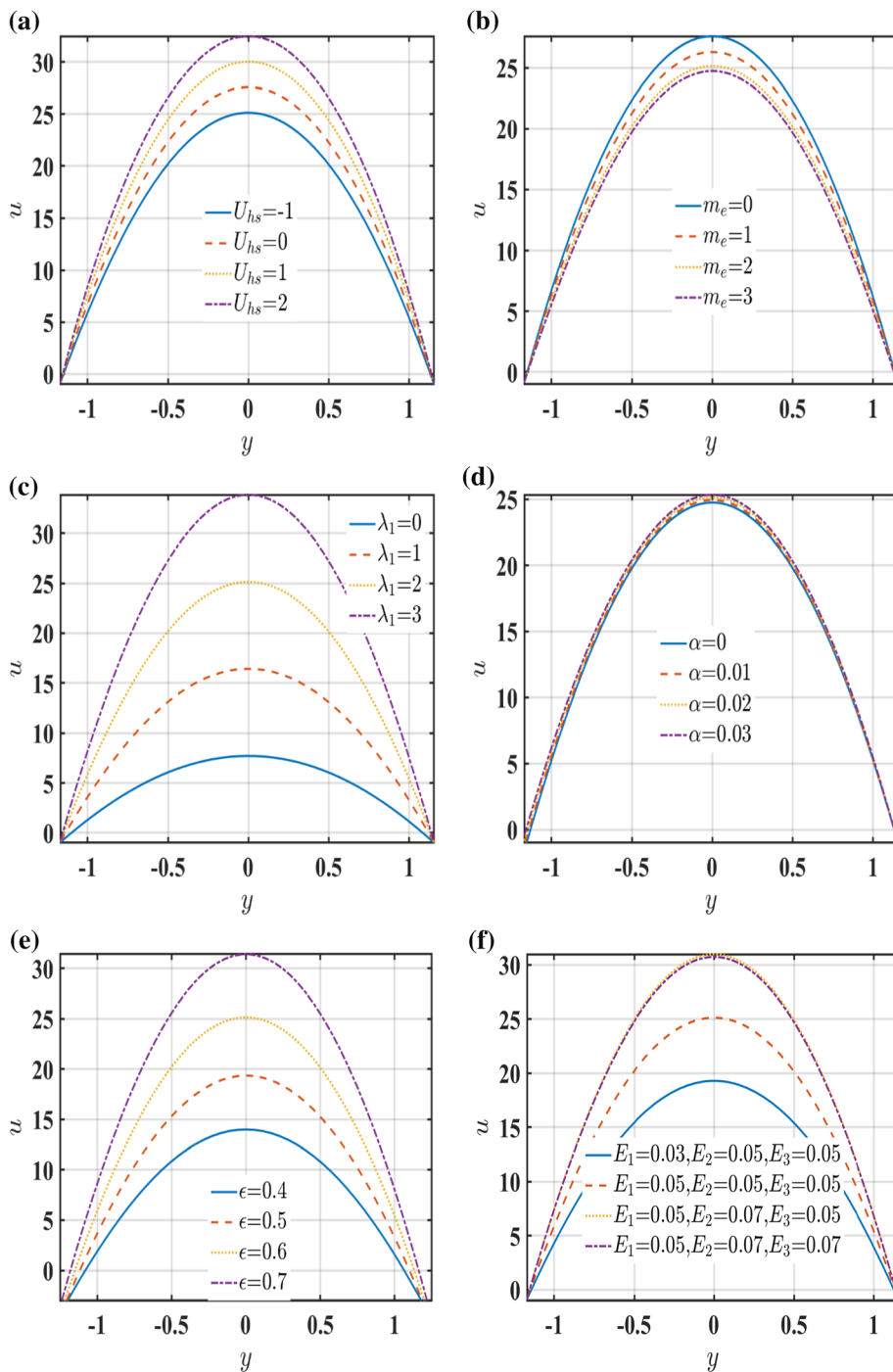
This part emphasizes on the impact of Helmholtz–Smoluchowski/maximum electro-osmotic velocity (U_{hs}), electro-osmotic parameter (m_e), Jeffrey parameter (λ_1), variable viscosity (α), amplitude ratio (ϵ), elasticity parameter (E_1), mass parameter (E_2), viscous damping force parameter (E_3), variable thermal conductivity (β), Brinkmann number (Br), Schmidt number (Sc) and Soret number (Sr) over stream line (ψ), velocity (u), temperature (θ) and concentration (Ω). The outcomes are shown in Figs. 2–10.

Figure 2 illustrates the impact of relevant parameters over speed. The velocity profiles have a parabolic form because to an optimum speed in the channel's center. Figure 2a explains that as U_{hs} , or the optimal electro-osmotic velocity (or Helmholtz–Smoluchowski speed), rises from -1 to 4 , the axial motion has considerable momentum. For higher U_{hs} , a succeeding improvement in an axial electric field involves a considerable deceleration. The

motion is maintained and delayed with an important electrical field strength. Tripathi et al. [65] investigated a similar trend. Other critical values of m_e in Fig. 2b initially reduce the velocity profiles. In addition, there is a minor difference in velocity profiles for larger values. The joint of λ_D is the Debye–Hückel design. Since raised ion migration occurs as we budge away from the accused surface, reducing λ_D , i.e., augmenting Debye–Hückel parameter, is thought to rise electrical capacity. Consequently, λ_D is a vital manner criterion in controlling potential electrical distinction, which influences the axial speed field. Figure 2c is drawn for several values of λ_I . The velocity profile progresses as the λ_I augments, as exposed here. With taking $\lambda_1 = 0$, the finding reduces to Newtonian fluid. Figure 2d describes the impact of α on velocity distributions. The velocity profile improves for more considerable values of α . Since a boost in α terms reduces the liquid's viscosity and therefore enhances the liquid movement. Figure 2e exposes a rise in the velocity profiles for more considerable values of amplitude ratio. Amplitude ratio is the relation between wave amplitude to channel width. Hence, a boost in amplitude ratio significantly improves the velocity profiles. The impact of flexibility, mass parameter, and viscous damping force term is exposed in Fig. 2f. With an improvement in the flexibility parameter, the fluid viscosity weakens since the particle moves at higher speeds. As the mass per unit area, the liquid travel particles freely develop the speed uplift. Since damping operates to resist the circulation speed because of energy loss, a minimizing response is apprehended. Clinically, once blood walls are supple or the mass per unit area augments (as in blood capillaries), the switch of water, oxygen, and other nutrients turns into easy. The damping tends to react in contradictory ways.

Here, we scrutinize the influence of diverse stipulations on temperature evolutions. The temperature evolutions are parabolic, via a maximum temperature level in the center of the channel. The consequences of viscous dissipation, which increases the temperature in the middle of the conduit, may discuss these patterns. The viscosity of the fluid causes this event, which transforms kinetic energy in the fluid into heat energy in it. Figure 3a indicates that the temperature of the fluid augments via an enhance in the maximum electro-osmotic velocity. Thus, the temperature profile diminishes for rising Debye–Hückel term (See Fig. 3b). Figure 3c is plotted to observe the influence of the Jeffrey design over the temperature distribution. It indicates that temperature is an increasing function of the Jeffrey pattern. Figure 3d is plotted to observe the effect of β on the temperature distribution. β is the liquid's aptitude to release or protect heat to its locations. As an outcome, when β of the fluid in the canal is superior to the wall temperature, the liquid's thermal evaluation rises. The

Fig. 2 $u(y)$ for fluctuating (a) U_{hs} , (b) m_e , (c) λ_1 , (d) α , (e) ϵ , (f) $E_1 - E_3$



effect of α on temperature distribution is demonstrated in Fig. 3e. α increases the temperature profile, and when α amounts to absolutely zero, consistent viscosity may be derived. The liquid's α improves, the heat transports prospective eliminates and increases the temperature profile. Figure 3f shows that larger values of Br improve the temperature profile. It is through an argument that less heat conducts the viscous dissipation. Br illustrates dissipation intensity. Known that the wall temperature is convectively

adjusted, heat transports are just considered due of the effects of heat dissipation. A similar pattern is seen for increasing values of amplitude ratio (See Fig. 3g). It has been observed that the temperature level increase is seen for the rising importance of flexible stress and mass per unit is parameter. The opposite behavior is spotted for an increasing value of the viscous damping force parameter (See Fig. 3h).

Fig. 3 $\theta(y)$ for fluctuating (a) U_{hs} , (b) m_e , (c) λ_1 , (d) β , (e) α , (f) Br , (g) ϵ , and (h) $E_1 - E_3$

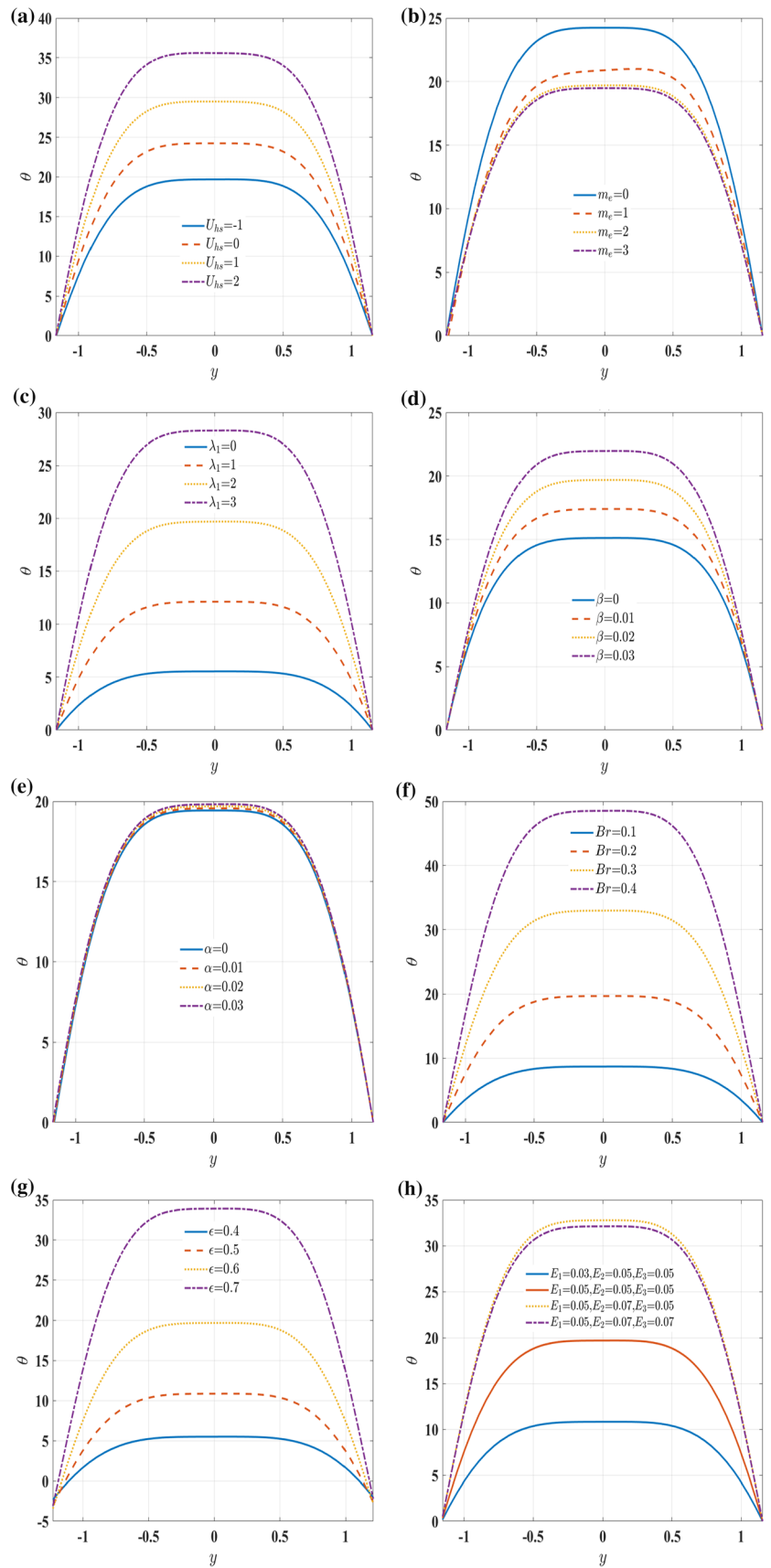


Fig. 4 $\Omega(y)$ for fluctuating (a) U_{hs} , (b) m_e , (c) λ_1 , (d) β , (e) α , (f) Br , (g) ϵ , and (h) $E_1 - E_3$

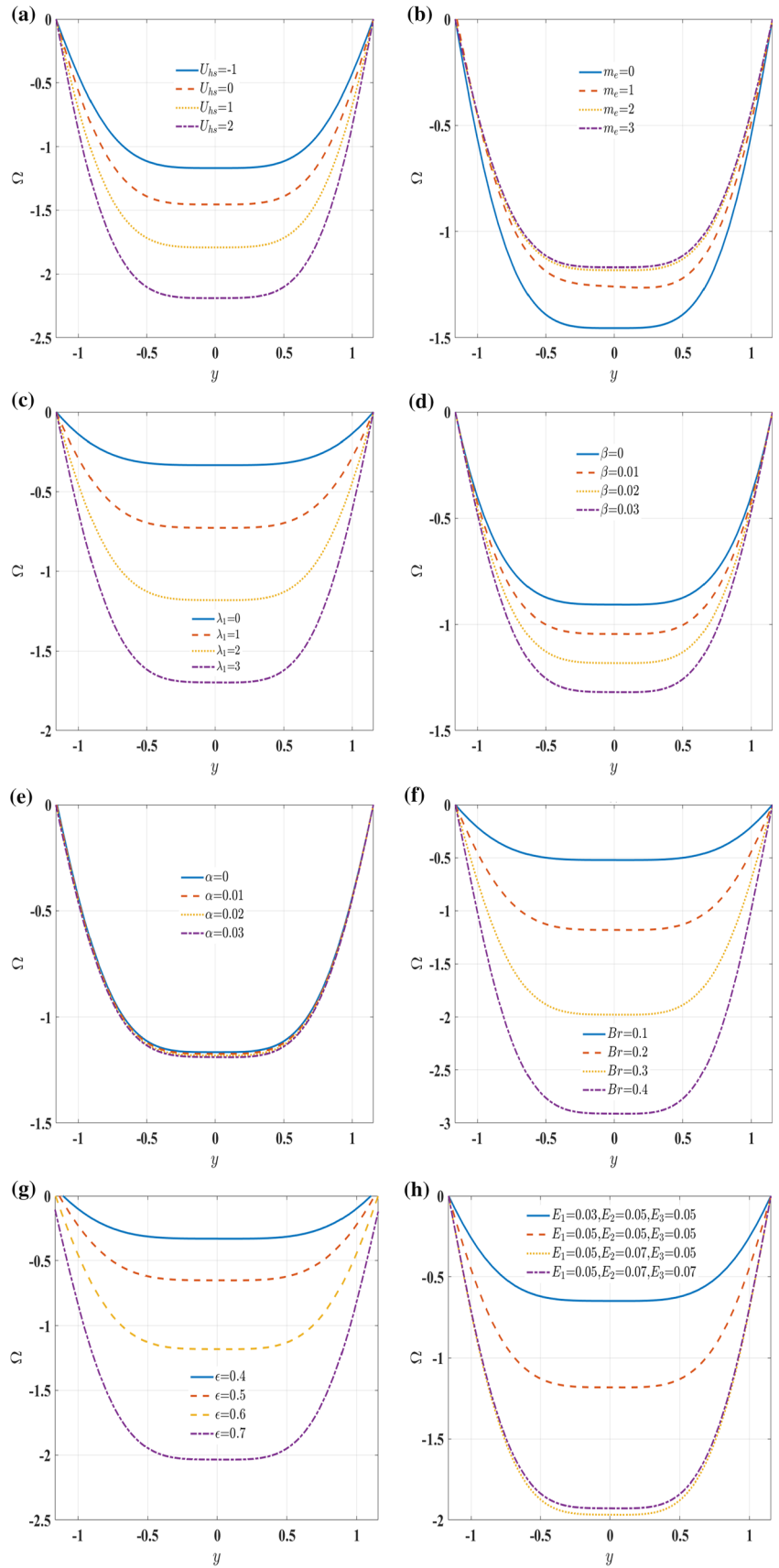


Fig. 5 $\Omega(y)$ for varying (a) Sc and (b) Sr

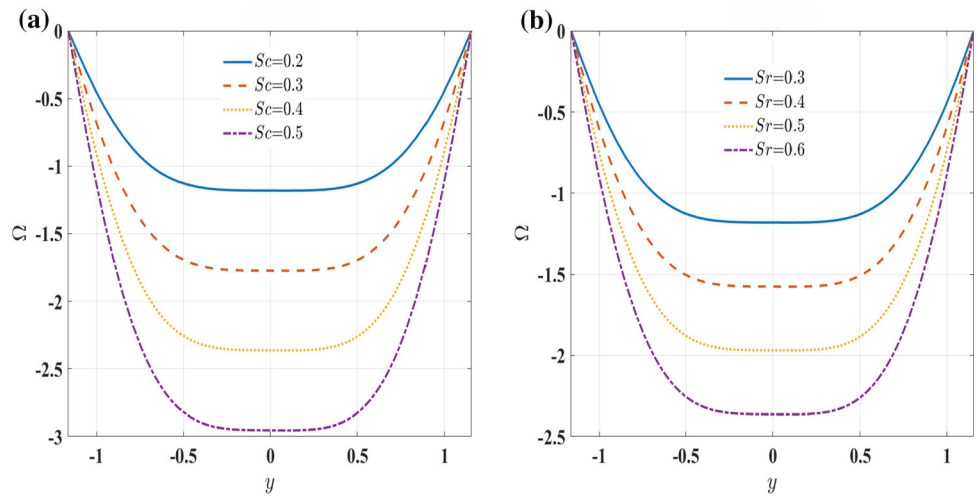
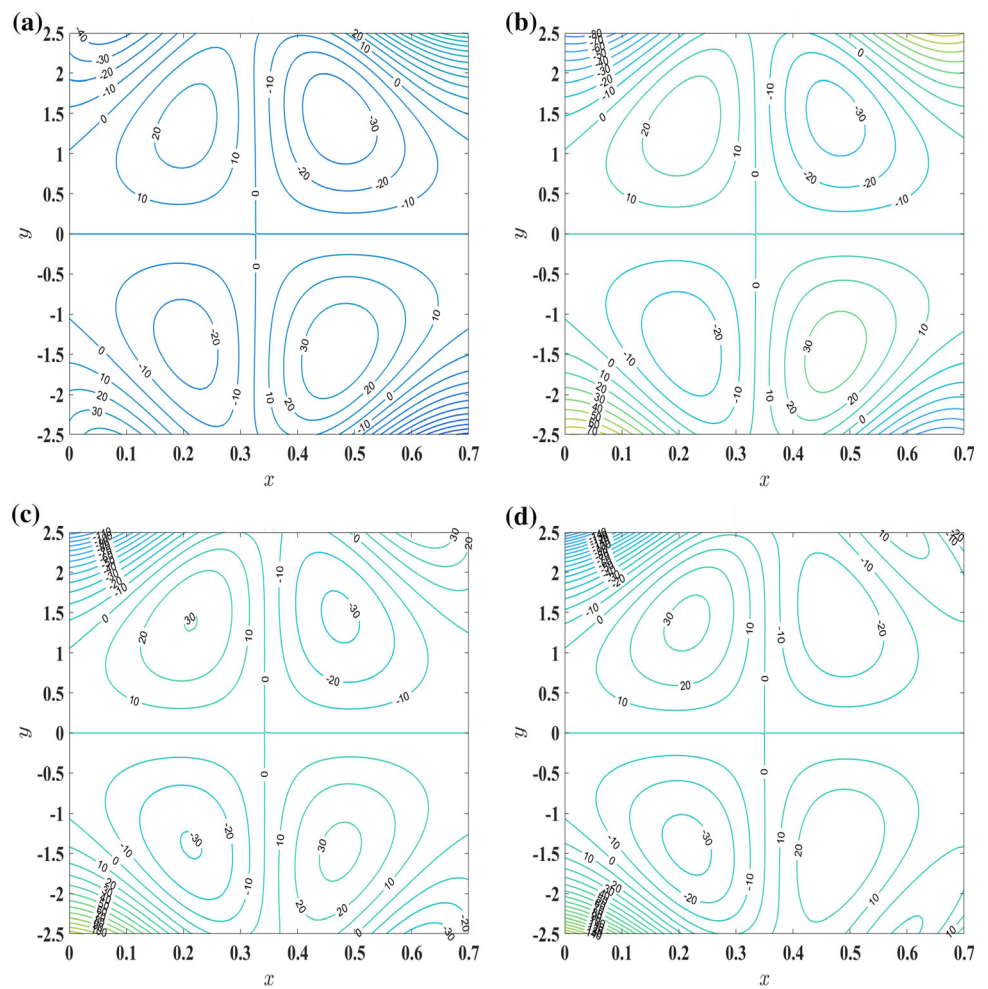


Fig. 6 $\psi(x, y)$ for varying (a) $U_{hs} = -1$, (b) $U_{hs} = 0$, (c) $U_{hs} = 1$, and (d) $U_{hs} = 2$



The repercussions of various criteria on concentration profiles are shown in Figs. 4 and 5. The concentration distribution behaves conflicting to that of temperature distribution in Fig. 4. This behavior is anticipated physically because heat and mass are known to be opposite to

straight proportion. Also, the profiles expose particle matter in the fluid that is more at the periphery than in the central position of the channel. This behavior assists in spreading necessary nutrients to nearby tissues and cells in the blood and other fluxes. Figure 5 is drawn to observe the

Fig. 7 $\psi(x, y)$ for varying (a) $m_e = 1$ and (b) $m_e = 3$

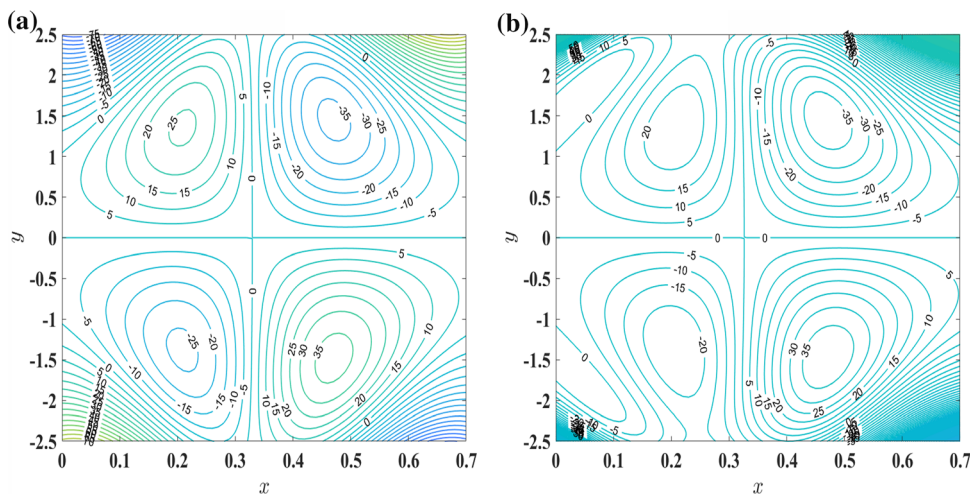


Fig. 8 $\psi(x, y)$ for fluctuating (a) $\lambda_1 = 0$ and (b) $\lambda_1 = 2$

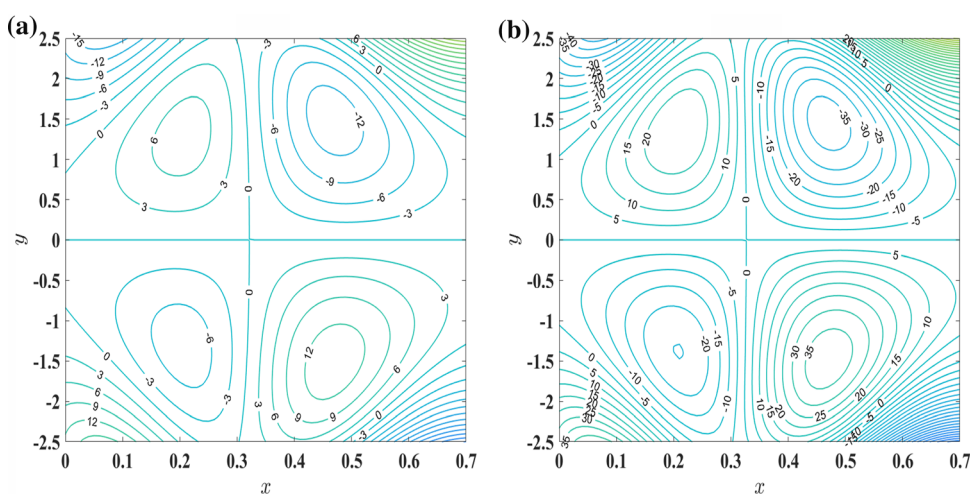
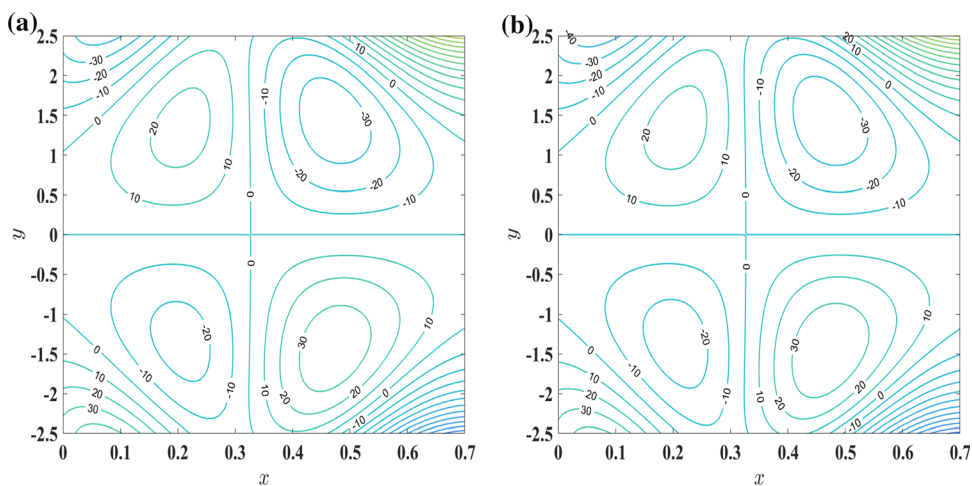


Fig. 9 $\psi(x, y)$ for varying (a) $\alpha = 0$ and (b) $\alpha = 0.02$



effect of Soret and Schmidt number on the velocity profiles. The figures reveal that the concentration profile substantially diminishes with an augment in the value of the Soret and Schmidt number.

It is usually known that the phenomenon of trapping is an integral element of peristaltic research studies. The liquid, therefore, caught within the bolus is pushed forward along through the peristaltic wave. Figure 6 shows a

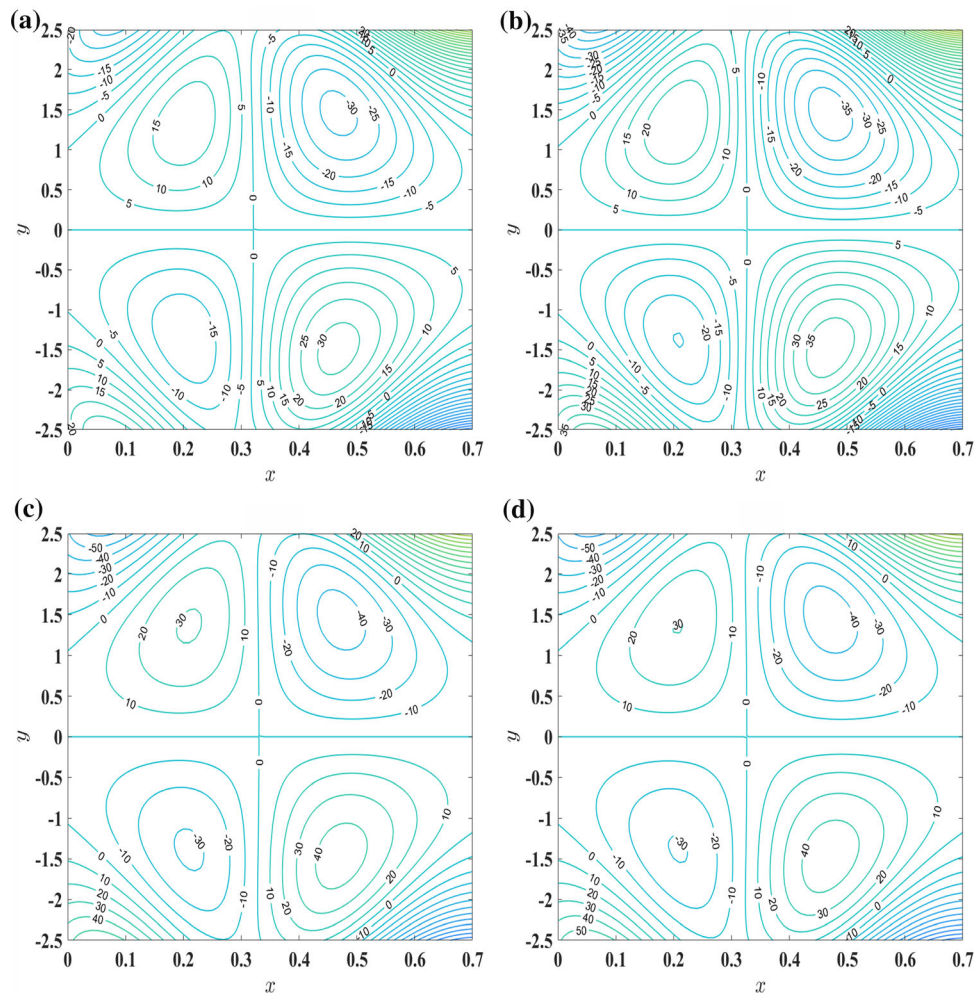


Fig. 10 $\psi(x, y)$ for varying (a) $E_2 = 0.05, E_3 = 0.05, E_1 = 0.03$, (b) $E_3 = 0.05, E_2 = 0.05, E_1 = 0.05$, (c) $E_1 = 0.05, E_2 = 0.07, E_3 = 0.05$, (d) $E_2 = 0.07, E_3 = 0.07, E_1 = 0.05$

streamlined makeup for various U_{hs} . It shows that the build-up of streamlines reduces through a rise in U_{hs} . Hence, stronger U_{hs} means a more powerful electrical field; the diversity of enclosed boluses considerably reduces for high values of U_{hs} . Figure 7 shows that the combination of enclosed boluses increases with arise in the electro-osmotic criterion. For greater m_e , the enclosed bolus appears stronger in EDL. Figure 8 illustrates the streamlines for varying Jeffrey specifications. It reveals that the streamlines considerably increase with arise in the value of the Jeffrey parameter. Similar behavior is noticed for a boost in the importance of α , flexible tension, mass per unit area, and viscous damping force parameter (See Figs. 9 and 10).

5. Conclusions

The influences of electro-osmotic, variable liquid properties, and wall properties toward the peristaltic flow of Jeffrey liquid via a uniform conduit are analyzed. MATLAB 2020a programming is utilized to confer the effect of critical expressions toward concentration, velocity, temperature level, and streamlines. The findings seen in this article have potential implications in both medical research and industry. Moreover, considering slip and changeable liquid properties in peristaltic movement, physical conditions such as a tapered/asymmetric uneven artery via a porous medium can be implemented in future research. This work gives a fair theoretical estimation for further research in this way. The main findings of the scheme are summarized as:

- The velocity profiles rise for larger values of optimum electro-osmotic velocity.
- The electro-osmotic specification is observed to be a reducing function of velocity.
- The Jeffrey criterion improves the temperature and velocity profiles.
- An increase in the velocity and temperature profiles is observed for increasing value of α .
- The temperature profile improves for more significant values of variable thermal conductivity.
- The concentration profile significantly diminishes for more significant values of Soret and Sc .
- The accumulation of streamlines reduces through a boost in maximum electro-osmotic velocity.
- The number of enclosed boluses increases through a boost in the electro-osmotic criterion.

References

- [1] T W Latham Fluid motions in a peristaltic pump *Master's Thesis, Massachusetts Institute of Technology, Cambridge* (1966)
- [2] K Raju and R Devantahan *Rheological Acta* **11** 170 (1972)
- [3] M Kothandapani and S Srinivas *International Journal of Non-linear Mechanics* **43** 915 (2008)
- [4] C Rajashekhar, G Manjunatha, K V Prasad, B B Divya and H Vaidya *Cogent Engineering* **5** 1495592 (2018)
- [5] S Srinivas, R Gayathri and M Kothandapani *Computer Physics Communication* **180** 2115 (2009)
- [6] D Tripathi *Journal of Fluids Engineering* **133** 121104 (2011)
- [7] M Gudekote and R Choudhari *Journal of Advanced Research in Fluid Mechanics and Thermal Sciences* **43** 67 (2018)
- [8] H Vaidya, M Gudekote, R Choudhari and K V Prasad *Multidisciplinary Modeling in Materials and Structures* **14** 940 (2018)
- [9] Z Abbas, M Y Rafiq, J Hasnain and T Javed *Arabian Journal for Science and Engineering* **46** 1997 (2021)
- [10] R Djebali, F Mebarek-Oudina and R Choudhari *Physica Scripta* **96** 085206 (2021)
- [11] O A Bég, T A Bég, R Bhargava, S Rawat and D Tripathi *Journal of Mechanics in Medicine and Biology* **12** 1250081 (2012)
- [12] A Alsaedi, N Ali, D Tripathi and T Hayat *Applied Mathematics and Mechanics* **35** 469 (2014)
- [13] D Tripathi, O A Beg, P K Gupta, G Radhakrishnamacharya and J Mazumdar *Journal of Bionic Engineering* **12** 643 (2015)
- [14] R P Sharma, M C Raju, S K Ghosh, S R Mishra and S Tinker *Indian Journal of Pure & Applied Physics* **58** 877 (2020)
- [15] G Kumaran, R Sivaraj, V R Prasad, O A Beg and R P Sharma *Physica Scripta* **96** 025222 (2021)
- [16] A K Verma, A K Gautam, K Bhattacharyya and R P Sharma *Sadhana* **46** 98 (2021)
- [17] P K Krishna, R P Sharma and N Sandeep *Nuclear Engineering and Technology* **49** 1654 (2017)
- [18] N Sandeep, R P Sharma and M Ferdows *Journal of Molecular Liquids* **234** 437 (2017)
- [19] R P Sharma, P Murthy and D Kumar *Journal of Nanofluids* **6** 80 (2017)
- [20] S Saranya, P Ragupathi, B Ganga, R P Sharma and A K A Hakeem *Advanced Powder Technology* **29** 1977 (2018)
- [21] R P Sharma, R Seshadri, S R Mishra and S R Munjam *Heat Transfer-Asian Research* **48** 2105 (2019)
- [22] S Jena, S R Mishra, P K Pattnaik and R P Sharma *Latin American Applied Research-An international Journal* **50** 283 (2020)
- [23] P S Rao, O M Prakash, S R Mishra and R P Sharma *Indian Journal of Geo-Marine Sciences* **49** 889 (2020)
- [24] S S Payad, N Sandeep and R P Sharma *Biointerface Research in Applied Chemistry* **11** 11499 (2021)
- [25] G Kumaran, R Sivaraj, V R Prasad, O A Beg and R P Sharma *Physica Scripta* **96** 025222 (2021)
- [26] Z M Mburu, S Mondal, P Sibanda and R Sharma *Journal of Thermal Engineering* **7** 845 (2021)
- [27] O D Makinde, M G Reddy and K V Reddy *Journal of Applied and Fluid Mechanics* **10** 1105 (2017)
- [28] K Das, R P Sharma and P R Duari *International Journal of Applied Mechanics and Engineering* **22** 827 (2017)
- [29] M G Reddy, K V Reddy and O D Makinde *International Journal of Applied and Computational Mathematics* **3** 3201 (2017)
- [30] P K Krishna, N Sandeep and R P Sharma *European Physical Journal Plus* **132** 202 (2017)
- [31] R P Sharma and S R Mishra *Measurement and control B* **87** 250 (2018)
- [32] R P Sharma, O D Makinde and I L Animasaun *Defect and Diffusion Forum* **387** 308 (2018)
- [33] R P Sharma, S M Ibrahim, M Jain and S R Mishra *Indian Journal of Pure and Applied Physics* **56** 732 (2018)
- [34] R P Sharma, M C Raju, O D Makinde, P R K Reddy and P C Reddy *Defect and Diffusion Forum* **392** 1 (2019)
- [35] R P Sharma, S Tinker, B J Gireesha and B Nagaraja *International Journal of Applied Mechanics and Engineering* **25** 103 (2020)
- [36] R P Sharma and S R Mishra *International Journal of Fluid Mechanics Research* **47** 121 (2020)
- [37] K Das, R P Sharma and A Sarkar *Journal of Computational Design and Engineering* **3** 330 (2016)
- [38] I Chabani, F Mebarek-Oudina and A A I Ismail *Micromachines* **13** 224 (2022)
- [39] R P Sharma, N Acharya and K Das *Indian Journal of Geo-Marine Sciences* **49** 641 (2020)
- [40] S Tinkera, S R Mishra and R P Sharma *Indian Journal of Pure and Applied Physics* **58** 558 (2020)
- [41] S Marzougui, F Mebarek-Oudina, M Magherbi and A Mchirgui *International Journal of Numerical Methods for Heat & Fluid Flow* (2021) <https://doi.org/10.1108/HFF-04-2021-0288>
- [42] R P Sharma, N Indumati, S Saranya, B Ganga and A K A Hakeem *Journal of The Indian Mathematical Society* **87** 261 (2020)
- [43] M M Khader and R P Sharma *Mathematics and Computers in Simulation* **181** 333 (2021)
- [44] A Shafiq, F Mebarek-Oudina, T N Sindhu and A Abidi *The European Physical Journal Plus* **136** 407 (2021)
- [45] K Swain, F Mebarek-Oudina and S M Abo-Dahab *Journal of Thermal Analysis and Calorimetry* **147** 1561 (2022)
- [46] A S Warke, K Ramesh, F Mebarek-Oudina and A Abidi *Journal of Thermal Analysis and Calorimetry* (2021) <https://doi.org/10.1007/s10973-021-10976-z>
- [47] S M Abo-Dahab, M A Abdelhafez, F Mebarek-Oudina and S M Bilal *Indian Journal of Physics* **95** 2703 (2021)
- [48] T Hayat, N Ali and S Asghar *Acta Mechanica* **193** 101 (2007)
- [49] N Sher, S Nadeem and C Lee *Results in Physics* **3** 152 (2013)
- [50] Q Hussain, S Asghar, T Hayat and A Alsaedi *Applied Mathematics and Mechanics* **36** 499 (2015)

- [51] B B Divya, G Manjunatha, C Rajashekhar, H Vaidya and K V Prasad *Alexandria Engineering Journal* **59** 693 (2020)
- [52] S Hamrelaine, F Mebarek-Oudina and M R Sari *Journal of Advanced Research in Fluid Mechanics and Thermal Sciences* **58** 173 (2019)
- [53] S Chakraborty *Journal of Physics D: Applied Physics* **39** 5356 (2006)
- [54] A Bandopadhyay, D Tripathi and S Chakraborty *Physics of Fluids* **28** 052002 (2016)
55. X Guo and H Qi *Micromachines* **8** 341 (2017)
- [56] S Waheed, S Noreen and A Hussanan *Applied Sciences* **9** 2164 (2019)
- [57] S Waheed, S Noreen, D Tripathi and D Lu *Journal of Biological Physics* **46** 45 (2020)
- [58] S Noreen, S Waheed, D C Lu and D Tripathi *International Communication in Heat and Mass Transfer* **123** 105180 (2021)
- [59] G H Tang, X F Li, Y L He and W Q Tao *Journal of Non-Newtonian Fluid Mechanics* **157** 133 (2009)
- [60] D Tripathi, A Yadav and O A Béq *The European Physical Journal Plus* **132** 173 (2017)
- [61] O A Béq, D Tripathi and A Sharma *International Journal of Heat and Mass Transfer* **111** 138 (2017)
- [62] D Tripathi, A Yadav, O A Béq and R Kumar *Microvascular Research* **117** 28 (2018)
- [63] D Tripathi, A Sharma and O A Béq *Advanced Powder Technology* **29** 639 (2018)
- [64] J Prakash, A Sharma and D Tripathi *Journal of Molecular Liquids* **249** 843 (2018)
- [65] D Tripathi, A Sharma and O A Béq *Advanced Powder Technol.* **29** 639 (2018)
- [66] D Tripathi, R Jhorar, O A Béq and S Shaw *Meccanica* **53** 2079 (2018)
- [67] J Prakash, K Ramesh, D Tripathi and R Kumar *Microvascular Research* **118** 162 (2018)
- [68] R Jhorar, D Tripathi, M M Bhatti and R Ellahi *Indian Journal of Physics* **92** 1229 (2018)
- [69] S Noreen and Q D Tripathi *Thermal Science and Engineering Progress* **11** 254 (2019)
- [70] V K Narla and D Tripathi *Microvascular Research* **123** 25 (2019)
- [71] S Hussain, N Ali and K Ullah *Rheological Acta* **58** 603 (2019)
- [72] N Ali, S Hussain, K Ullah and O A Béq *The European Physical Journal Plus* **134** 141 (2019)
- [73] A Sharma, D Tripathi, R K Sharma and A K Tiwari *Physica A: Statistical Mechanics and its Applications* **535** 122148 (2019)
- [74] S Noreen, S Waheed, D C Lu and A Hussanan *Alexandria Engineering Journal* **59** 4081 (2020)
- [75] D Tripathi, J Prakash, M G Reddy and J C Misra *Journal of Thermal Analysis and Calorimetry* **143** 2499 (2021)
- [76] D Tripathi, J Prakash, M G Reddy and R Kumar *Indian Journal of Physics* **95** 2411 (2021)
- [77] N Ali, Q Hussain, T Hayat and S Asghar *Physics Letters A* **372** 1477 (2008)
- [78] S Nadeem, T Hayat, N S Akbar and M Y Malik *International Journal of Heat and Mass Transfer* **52** 4722 (2009)
- [79] T Hayat, M I Khan, M Farooq, A Alsaedi, M Waqas and T Yasmeen *International Journal of Heat and Mass Transfer* **99** 702 (2016)
- [80] H Vaidya, C Rajashekhar, G Manjunatha and K V Prasad *The European Physical Journal Plus* **134** 231 (2019)
- [81] G Manjunatha, C Rajashekhar, H Vaidya, K V Prasad, O D Makinde and J Viharika *Arabian Journal for Science and Engineering* **45** 417 (2020)
- [82] H Vaidya, C Rajashekhar, G Manjunatha and K V Prasad *Journal of Brazilian Society of Mechanical Science and Engineering* **41** 52 (2019)
- [83] Y M Chu et al *International Communication in Heat and Mass Transfer* **119** 104980 (2020)
- [84] B B Divya, G Manjunatha, C Rajashekhar, H Vaidya and K V Prasad *Ain Shams Engineering Journal* **12** 2181 (2021)
- [85] H Vaidya, C Rajashekhar, K V Prasad, S U Khan, F Mebarek-Oudina, A Patil and P Nagathan *SN Applied Sciences* **3** 186 (2021)
- [86] M M Rahman, H F Öztop, R Saidur, S Mekhilef and K Al-Salem *Computers & Fluids* **79** 53 (2013)
- [87] F Selimefendigil and H F Öztop *International journal of heat and mass transfer* **108** 156 (2019)
- [88] H Vaidya, C Rajashekhar, K V Prasad, S U Khan, A Riaz and J Vihariaka *Biomechics and Modelling in Mechanobiology* **20** 1047 (2021)
- [89] C Rajashekhar, F Mebarek-Oudina, H Vaidya, K V Prasad, G Manjunatha and H Balachandra *Heat Transfer-Asian Research* **50** 5106 (2021)

Publisher's Note Springer Nature remains neutral with regard to jurisdictional claims in published maps and institutional affiliations.